Different Active Sites of $LaCoO_3$ and $LaMnO_3$ for CH_4 Oxidation by Regulation of Precursor's Ion Concentration

Saifei Wang[1], Yiyuan Zhang[1], Peiqi Chu[1], Jie Liu[1], Man Wang[1], Peng Zhang[2] and Erhong Duan[1,*]

[1]School of Environmental Science and Engineering, Hebei University of Science and Technology, 26th Yuxiang Street, Shijiazhuang Hebei, 050018, and [2]Hebei NCPC Environment Protection & Research Co., Ltd, Shijiazhuang, Hebei, 050015, PR China

Abstract: Pure $LaCoO_3$ and $LaMnO_3$ were synthesized under different ion concentrations of precursors and the difference of active sites for CH_4 oxidation between them was found. As the ion concentration of precursors increased, the two kind of perovskite crystals grew larger along with agglomerate. Meanwhile, $LaCoO_3$ and $LaMnO_3$ prepared by high ion concentrations of precursors enriched more surface Co^{3+} or Mn^{4+}. The catalytic activity of the catalysts was tested in the oxidation reaction of methane under fuel-lean condition, results showed that LC-1.0 and LM-2.0 had the optimal activity and the light-off temperatures were 492°C and 486°C, respectively. Combining the physical and chemical characterization, the $LaCoO_3$ and $LaMnO_3$ possess different active sites for the methane catalytic reaction, and the conclusion was further verified by the DFT simulation. For $LaCoO_3$, the surface lattice oxygen is the main active site, while for $LaMnO_3$, the reaction is facilitated by the high-valent manganese.

Keywords: Perovskite; Methane oxidation; Active sites; DFT simulation.

1. INTRODUCTION

Fuel-lean methane gas (0.1-1 vol% CH_4) is mainly emitted from natural gas vehicles and typical gassy mines [1,2].The direct emission of fuel-lean methane gas is not only a waste of green energy, but also as greenhouse gas to pollute the environment [3,4]. The abatement of methane atmospheric emissions has become one of the important challenges of environmental protection [5,6]. In recent years, many attempts have been done to drop the harmful environmental effect of methane release, such as catalytic oxidation.

The catalysts for methane oxidation have been conducted involving precious metals Pd, Au, and Ag supported on various oxides, including ZrO_2, Al_2O_3, CeO_2[7-9].Although the empty conduction d-bands of precious metals could readily activate C-H bonds of methane [10], high-cost and decomposition of active component at high temperature severely restrict their long-term application [11]. Durable oxidation and economic effective catalysts have become critical for cutting fuel-lean methane gas.

In addition to precious metal catalysts, perovskite-type oxides (ABO_3) are known for their chemical flexibility and wide range of industrial applications [6,12-13]. The A and B sites can be replaced by other metal ions with similar atomic radii to achieve more surface defects and higher activity [14]. Generally, lanthanum-based perovskite (A site is lanthanum) possess considerable activity in methane oxidation, CO and soot [15]. Transition metal cations on B-site with multiple valence states play a decisive role in the methane catalytic oxidation [16]. Among them, $LaCoO_3$ and $LaMnO_3$, are recognized as two kinds of perovskites with excellent activity and have been extensively studied [17].

Compared with the catalytic oxidation mechanism of CH_4 on precious metals and their supported oxides, the mechanism of CH_4 oxidation on different perovskite catalysts is still controversial. Research has shown that the oxidation activity of perovskite oxides is related to the change in the oxidation state between adjacent transition metal ions [18], revealing that fundamental difference exists between $LaCoO_3$ and $LaMnO_3$ [19]: the redox couple for $LaCoO_3$ is Co^{3+}/Co^{2+}, while for $LaMnO_3$, it is Mn^{4+}/Mn^{3+} for methane catalytic combustion. Porta *et al*. [20] observed the variations of the electrical conductivity of the $LaCoO_3$ and $LaMnO_3$ during the processes of oxygen adsorption-desorption. They found that oxygen firmly fixed on the surface of $LaCoO_3$ and was difficult to remove. On the contrary, for $LaMnO_3$, the rate of oxygen desorption is higher than that of oxygen adsorption. They also gave the conclusion that oxygen is less easily fixed on the surface and more easily oxidized by Mn^{4+} ions on the surface of $LaMnO_3$. Although this difference was established experimentally by many studies, the

*Address correspondence to this author at the School of Environmental Science and Engineering, Hebei University of Science and Technology, 26th Yuxiang Street, Shijiazhuang Hebei, 050018, PR China; Tel: +0311-8166-6524; duan_eh@163.com

E-ISSN: 2410-3624/20

fundamental questions for active sites of $LaCoO_3$ and $LaMnO_3$ are still up in the air. Overall, the methane catalytic activity of perovskites is, however, affected by the surface lattice oxygen and by the adsorbed oxygen species on oxygen vacancies [21], which directly depends on their surface component and structural properties [22].

The surface and structural properties of the perovskites are highly dependent on the method of preparation. The synthesis of perovskites is often conducted by solid state, co-precipitation, sol-gel, solution combustion and hydrothermal method [23-27]. Among them, the sol-gel technique is widely employed because it can keep the cations homogeneously dispersed and mixed at a molecular level [23]. In the sol-gel method, the reactant ions are hydrolyzed and polymerized, and then condensed into sol or gel, and finally calcined to obtain a perovskite. Since the characteristic of precursor aqueous solution can reflect the general crystal form and particle distribution of the targeted perovskite, researchers can obtain a specific structure by controlling the precursor solution.

In this work, we employed sol-gel method to synthesized $LaCoO_3$ and $LaMnO_3$ perovskites [28], by simply adjusted the ion concentration of precursors, we obtained two series of perovskites with different textural properties. The structural and morphological properties were characterized by scanning electron microscopy (SEM) and X-ray diffraction (XRD). Their performance in catalytic oxidation of fuel-lean methane was measured by evaluation device. Meanwhile, the redox ability and surface species of the catalysts were examined by temperature programmed reduction (H_2-TPR) and X-ray Photoelectron Spectroscopy (XPS), respectively. The actual reaction process of methane was identified by *in situ* diffuse reflectance infrared Fourier transform spectroscopy (*in situ* DRIFTS) and Density Functional Theory (DFT) calculation. Structure-activity relationship was established through the above characterization, and the active site of $LaCoO_3$ and $LaMnO_3$ perovskites was also confirmed. Characterization and kinetics studies of the two perovskites convincingly indicate that there are very different catalytic processes between $LaCoO_3$ and $LaMnO_3$.

2. MATERIALS AND METHODS

2.1. Reagents

All the reagents were A.R. grade and were directly used. Lanthanum nitrate ($La(NO_3)_3{\cdot}6H_2O$, 99.0%), cobalt nitrate ($Co(NO_3)_2{\cdot}6H_2O$, 99.0%), Manganese nitrate ($Mn(NO_3)_2$, 50.0%), and citric acid ($C_6H_8O_7{\cdot}H_2O$, 99.0%) were purchased from Sinopharm Chemical Reagent Co. Ltd., (Shanghai, China). Ultrapure water (18.2 MΩ*cm) was used to prepare the solutions in all experiments.

2.2. Preparation of $LaCoO_3$ and $LaMnO_3$ Perovskites

Stoichiometric amounts of metal nitrate and citric acid were added to deionized water based on the molar ratio (La+Co or La+Mn): citric acid = 1:1.2. The precursor solution was continuously stirred at 80°C until it was dried. The viscous mixture was decomposed at 400°C for 0.5h and then grinded and calcined at 500°C for 1h to remove the remaining citric acid. Finally, the solid powder was calcined at 800°C for 5h to form perovskite crystal phase.

The viscous mixture experienced pre-calcination at 400°C for 0.5h followed by calcination at 500°C for 1h to remove the remaining citric acid, and finally 800°C for 5 h to form the perovskite crystal phase. The ion concentration of (La+Co or La+Mn) ranged from 0.1 mol/L to 2.0 mol/L, which was recorded as LC-*x* or LM-*x*. The exact element content of LC-x and LM-x catalysts are shown in Table **1**.

2.3. Characterization

The crystal structure was determined by an X-ray diffraction analysis, which was performed on an X-ray diffraction (D/MAX-2500, Rigaku) that was operated with Cu K*α* radiation. The Brunauer-Emmett-Teller (BET) surface areas of the catalysts were performed by nitrogen sorption at liquid nitrogen temperature (77 K) using a Quantachrome Autosorb iQ instrument. The catalysts were degassed at 473 K for 4 h to remove any residual moisture and other volatiles before N_2 adsorption. The morphologies and structures were observed by scanning electron microscopy (SEM, HITACHI S-4800). The X-ray photoelectron spectroscopy (XPS) spectra were recorded on an AXIS-Ultra-DLD spectrometer using Al Kα as an excitation source. The binding energy (BE) scale was calibrated by measuring the C1s peak (BE=284.8eV) from the ubiquitous surface layer of adventitious carbon. The temperature-programmed reduction of the H_2 (H_2-TPR) experiments were carried out by a conventional flow system equipped with a thermal conductivity detector (TCD). For the H_2-TPR analysis, 100mg sample was first pretreated under He flow (20 mL/min)and the temperature was increased to 350°C (a ramp rate of

Table 1: The Exact Element Content of the LC-x and LM-x Catalysts were Measured by ICP

Catalysts	La(%)	Co(%)	Mn(%)	La / Co	La /Mn
LC-0.5	0.41	0.40	-	1.0	-
LC-1.0	0.41	0.40	-	1.0	-
LC-1.5	0.40	0.39	-	1.0	-
LC-2.0	0.42	0.41	-	1.0	-
LM-0.1	0.42	-	0.36	-	1.2
LM-0.2	0.41	-	0.37	-	1.1
LM-0.5	0.40	-	0.37	-	1.1
LM-1.0	0.40	-	0.38	-	1.1
LM-1.5	0.39	-	0.38	-	1.0
LM-2.0	0.40	-	0.39	-	1.0

10°C/min), then the temperature was kept at 350°C for 60 min. A 5% H_2 (N_2 as the balance gas) was introduced(30 mL/min) at RT for 30min, followed by He at 20 mL/min for 30 min. A temperature-program from RT to 900°C with a ramp rate of 10°C/min was conducted and the H_2 concentration in the effluent stream was recorded by TCD. *In situ* diffuse reflectance infrared Fourier-transform spectroscopy (DRIFTS) was undertaken using a Thermo scientific IS50 FTIR spectrometer equipped with a liquid N_2-cooled MIR source, KBr optics, and Rock Solid interferometer.

DFT simulation details: The geometrical optimization and electronic properties of the $LaCoO_3$/$LaMnO_3$surface and the CH_4/CH_3/COOH radicals absorbed on those surfaces were calculated under the theory of density functional theory (DFT), and using the Vienna ab initio simulation package (VASP) [29,30]. The projector augmented wave (PAW) potentials were used as pseudo potentials to describe the interactions between the valence electrons and ions. The Perdew-Burke-Ernzerh (PBE) function of generalized gradient approximation (GGA) was used to describe the exchange-correlation of valence electrons [31].The optimized lattice parameters of $LaCoO_3$ were 3.823°C x 3.823°C x 3.823°C, and 3.903°C x 3.903°C x 3.903°C x for $LaMnO_3$. The optimization simulations were performed using a conjugate gradient algorithm with a force tolerance of 0.01 eV/Å, and the kinetic energy cut-off set at 500 eV under a Gamma k-point sampling of 7 ×7 ×7; The $LaCoO_3$ and $LaMnO_3$ surface model was built by cutting (110) from unit cells in bulk structure, and a 2×2 supercell was created. The surface model contains 4 La layers in the z-direction and the optimization process was performed by using a conjugate gradient algorithm with a force tolerance of 0.02 eV/Åand the kinetic energy cutoff was set as 500 eV. The 3 outermost layers of atoms were free to move, while the atoms of the inner layers were fixed. A Gamma k-point sampling of 5 ×5 ×1 was used for both the $LaCoO_3$ (110) surface and the $LaMnO_3$ (110) surface. Dipole corrections were applied to the z-direction to remove any possible net dipole moments.

2.4. Catalytic Activity Measurements

The catalytic performance was measured in a fixed-bed tubular stainless steel reactor (diameter of 10mm) under atmospheric pressure. The reaction gas composition (volume fraction) was 1% CH_4, 99% mixed air with a speed of 100 mL/min, and it was controlled by a mass flow controller (accuracy: 1.5%). The stainless steel reactor was loaded with 1mL sample (40-60 mesh, catalyst bed depth of 10mm). The concentration inlet and outlet of methane were analyzed by gas chromatography (Tian Mei, GC7900, China) with a flame ionization detector (FID), and TDX-01 molecular sieve column (2 m×3 mm, 80 mesh). The methane conversion *y*% was defined as:

$$y\%=[(C_0-C_1)/C_0]\times 100\% \quad (1)$$

Where C_0 and C_1 are the molar concentration of inlet and outlet methane and *y*% is the conversion of methane.

3. RESULTS AND DISCUSSION

3.1. Structural and Textural Properties

The X-ray diffraction patterns for $LaCoO_3$ and $LaMnO_3$ catalysts by different ion concentrations of precursors were presented in Figure **1**. For LC-*x*, when

x was lower than 0.5, the catalysts contained mixed phases of La_2O_3 (PDF#01-071-5408) and $LaCoO_3$ (PDF#01-048-0123) perovskite-type oxides; When x rose above 0.5, the catalysts only existed as a single crystal phase of $LaCoO_3$. For LM-*x*, a pure $LaMnO_3$ phase was obtained for all concentration of precursors, which were fitted with orthorhombic structures of $LaMnO_{3+\delta}$ (PDF#01-075-3213). The crystal domain size (D) was calculated by the Debye-Scherrer formula and listed in Table **2**. The results showed an increase in the crystal domain size with an increase of the precursors ion concentration for pure $LaCoO_3$ and $LaMnO_3$ catalysts, which may be attributed to the fine crystalline of perovskite crystal under high ion concentration of precursors.

The specific surface areas (SSA) of pure catalysts were also obtained and listed in Table **2**. The SSA values of all the catalysts were rather low due to high-temperature calcinations, but the SSA of LM-x was higher than that of LC-x in general. There was a negative correlation between the specific surface area and the ion concentration of precursors. Indeed, larger crystal domain size from the high ion concentration of precursors may cause a decrease in the specific surface area, which can also be reflected in the microscopic morphology of the catalysts. Figure (**S1**) displayed the nitrogen adsorption/desorption isotherms and pore size distributions of these catalysts. It was seen that all prepared catalysts presented a meso-porous structure with a pore size of approximately 3 nm. The morphologies of the pure perovskite oxides were investigated by SEM (see Figure **2**). Agglomerated ellipsoid nanocrystals were observed for the LC-x catalysts with a particle size of approximately 200 nm (see Figure **2a-d**). As shown in Figure (**2e-j**), LM-x catalysts possessed a lower particle size of approximately 100 nm compared with the LC-x catalysts, which was accordance with the BET results. However, with the increase in the precursor ion concentrations,

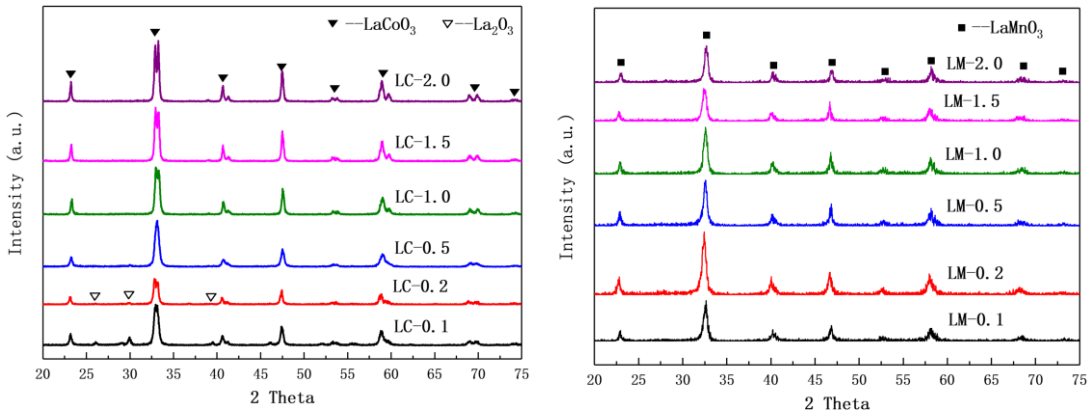

(**a**) (**b**)

Figure 1: XRD patterns of different precursors ion concentration of (a) LC-x and (b) LM-x catalysts.

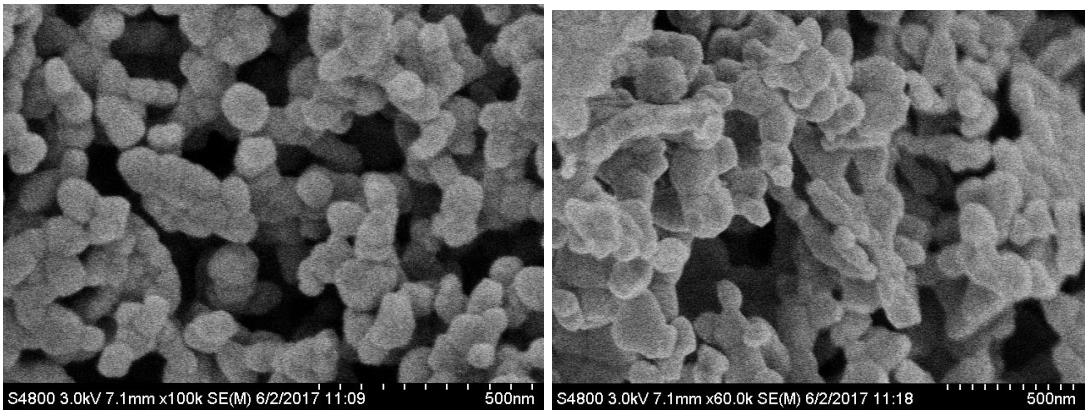

(**a**) (**b**)

Figure 2: (contd….)

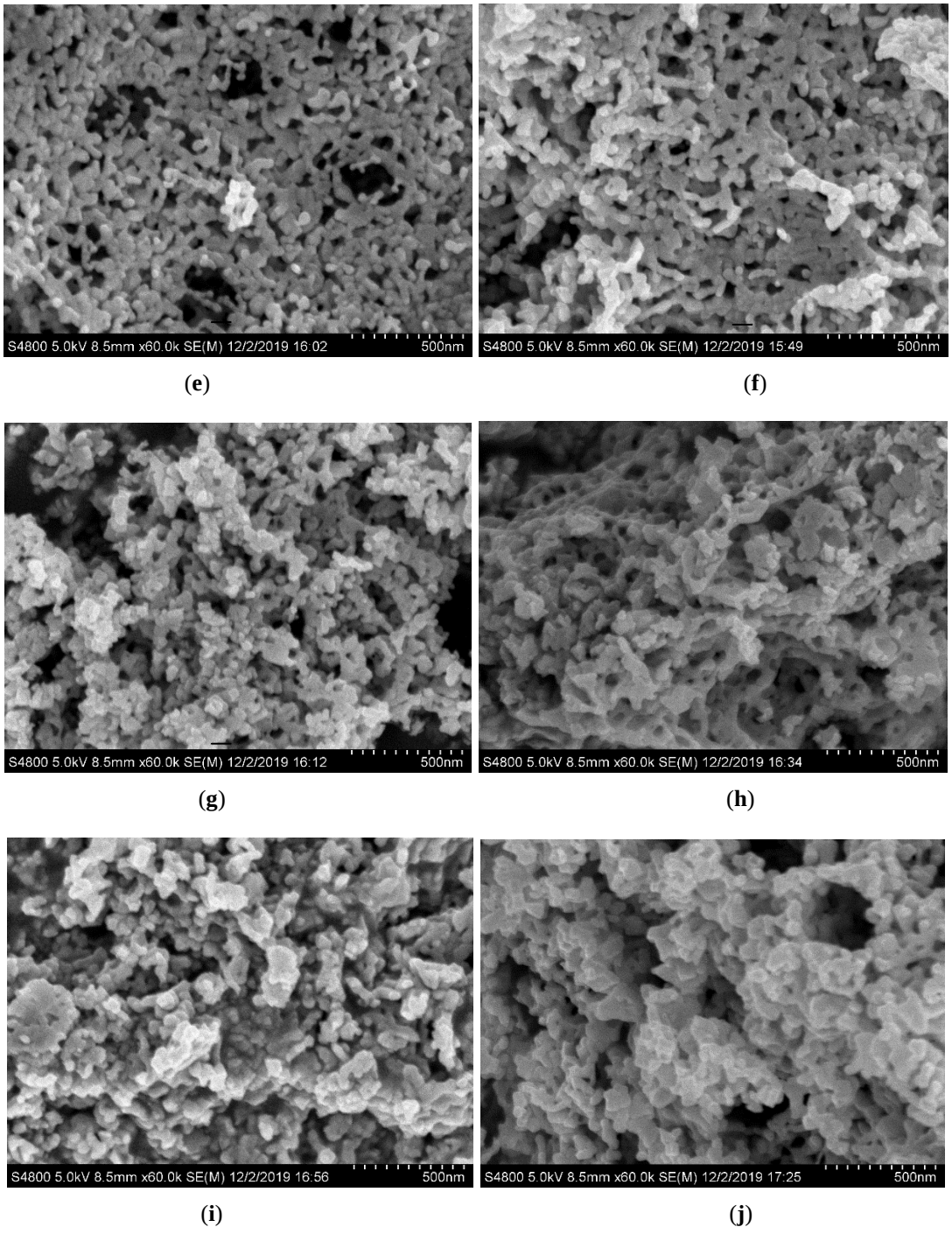

Figure 2: SEM images of (**a**) LC-0.5, (**b**) LC-1.0, (**c**) LC-1.5, (**d**) LC-2.0, (**e**) LM-0.1, (**f**) LM-0.2, (**g**) LM-0.5, (**h**) LM-1.0, (**i**) LM-1.5, (**j**) LM-2.0 catalysts.

the pore was gradually filled, and the catalysts became more agglomerated.

3.2. Catalytic Properties for CH_4 Oxidation

The catalytic activity of CH_4 was determined for all pure perovskites (Figure **3**). Each catalyst showed a measurable activity above 300°C and reached a conversion of 90% at 800°C.The light-off temperature (T_{50}) expressed that 50% of the CH_4 conversion was reached. Relatively speaking, low precursors ion concentration of $LaCoO_3$ presented higher activity. The best one appeared in LC-1.0, for which $T_{50}$was 492°C, and the least active was LC-1.5, whose $T_{50}$was 611°C.

Table 2: Physical Properties and Catalytic Performance of LC-x and LM-x Catalysts

Catalysts	D (nm)	Pore Diameter (nm)	Pore Volume (cc/g)	SSA(m^2/g)	T_{50}(°C)
LC-0.5	25.3	3.83	0.06	8	544
LC-1.0	38.8	3.05	0.09	7	492
LC-1.5	44.1	2.19	0.05	6	611
LC-2.0	53.1	3.06	0.07	6	583
LM-0.1	21.3	3.06	0.18	17	728
LM-0.2	26.4	3.06	0.18	15	655
LM-0.5	28.4	3.05	0.12	14	537
LM-1.0	35.3	3.41	0.20	14	487
LM-1.5	35.5	3.05	0.20	15	513
LM-2.0	42.3	3.83	0.17	14	486

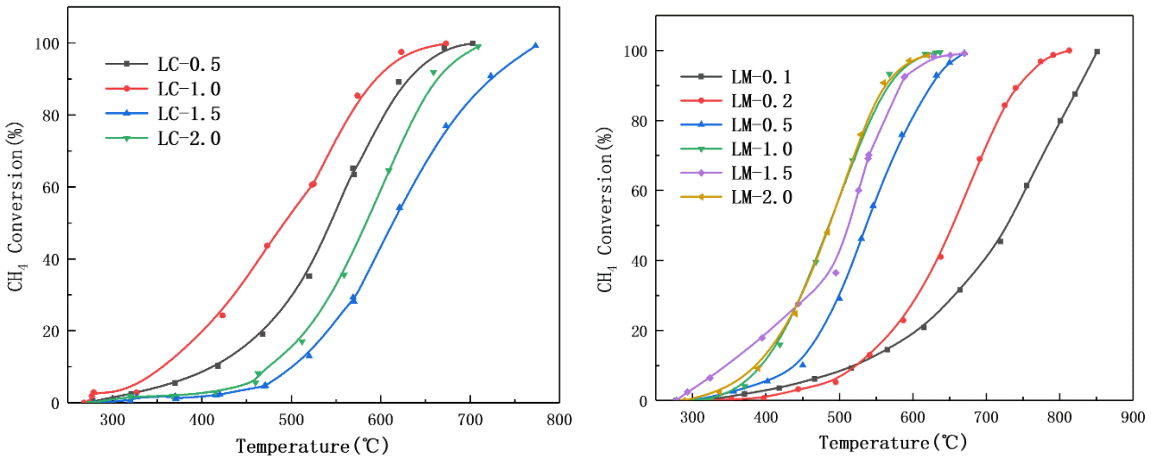

(**a**) (**b**)

Figure 3: Methane conversion as a function of reaction temperature for the as-prepared (**a**) LC-x and (**b**) LM-x catalysts.

In the case of LM-x, the best one was LM-2.0, for which the T_{50} was 486°C, and the least active was LC-0.1, for which the T_{50} was 736°C. High ion concentration of precursors beneficially improved the activity of $LaMnO_3$. Thus, the changes on ion concentration of the two series catalysts strongly influenced the catalytic activity of methane. In general, $LaMnO_3$ had a relatively lower T_{50} and better activity than $LaCoO_3$. Therefore, these two different trends suggested different activity sites between $LaCoO_3$ and $LaMnO_3$. Further research was performed to reveal the inherent differences.

3.3. Redox Ability

The optimal (LC-1.0 and LM-2.0) and worst (LC-1.5 and LM-0.1) activities of catalysts in two series were selected for the H_2-TPR (H_2-temperature programmed reduction) analysis (Figure **4**). The reduction profile of LC-x in Figure (**4a**) clearly showed two major peaks: the first one appeared below 500°C, and the other one was above 550°C. As reported before [32], the low-temperature peak (LTP) was caused by the reduction of Co^{3+} to Co^{2+} in the form of $LaCoO_{2.5}$. The high-temperature peak (HTP), related to the Co^{2+} to Co^0, represented the removal of bulk oxygen and eventually Co^0dispersed on La_2O_3. The reduction temperature of LC-1.0 was lower than that of LC-1.5, showing ideal redox ability as compared to LC-1.5. The H_2 consumption of LC-1.0 at high temperature was 0.65 mmol/g, which meant a higher amount of lattice oxygen.

The reduction profile of LM-x showed in Figure (**4b**) also showed two major groups of peaks: LTP below 500°C and HTP above 700°C. The LTP of LM-0.1 and LM-2.0 all contained two overlapping peaks which centered at 374°C, 447°C and 342°C, 421°C, respect-

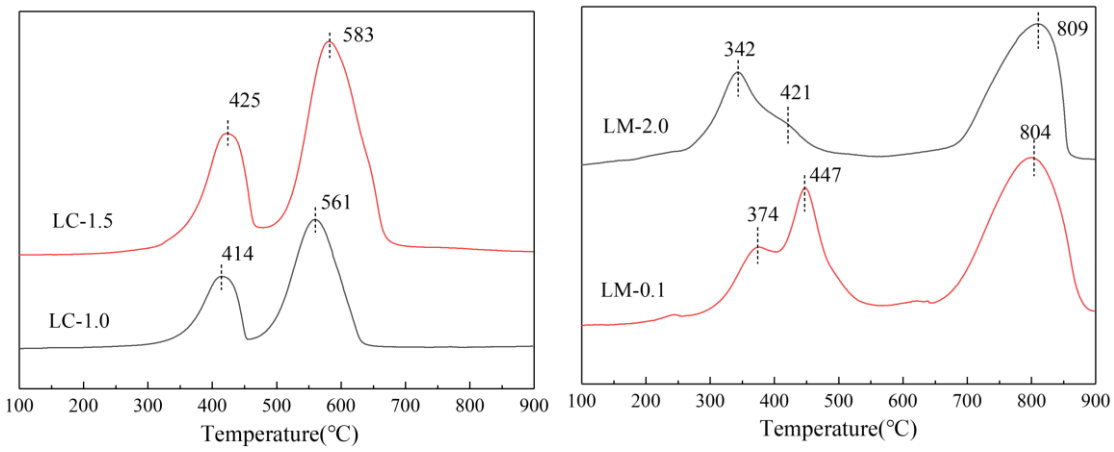

Figure 4: H_2-TPR profile of (**a**) LC-x and (**b**) LM-x catalysts.

ively. The lower one was caused by the reduction of high-valence Mn^{4+} to Mn^{3+}, and the higher one was derived from the reduction of surface Mn^{3+} to Mn^{2+}[33]. Obviously, LM-2.0possessed more Mn^{4+} and had better redox properties at low temperature than that of LM-0.1. The HTP corresponded to the reduction of the remaining Mn^{3+} to Mn^{2+} in the structure and the two samples had almost the same reduction temperature. By contrast, LM-x had a higher HTP than LC-x, and even above the catalytic temperature, it was revealed that the lattice oxygen, or say, the reduction of Mn^{3+} to Mn^{2+} in $LaMnO_3$ did not participate in the reaction. While the HTP of LC-1.0 and LC-1.5 appeared at 561°C and 583°C, this indicated that the lattice oxygen of $LaCoO_3$ participated in the catalytic reaction. Thus, the LC-1.0 possessed both lower LTP and HTP and had better activity than LC-1.5.

3.4. XPS Characterization

The valence states of B-site metals and the surface oxygen on catalysts were analyzed by XPS and are described separately (see Figure **5** and Table **3**). The spectra of Co_{2p} (Figure **5a**) can be divided into three categories according to the XPS data booklet: peaks ca. 779.6eV; 794.4eV corresponded to Co^{2+}, peaks ca.780.9eV, 796.2eV corresponded to Co^{3+}, and satellite peaks appeared at approximately 789.6eV [34]. Three component peaks were resolved for the spectra of $Mn_{2p\ 3/2}$in (Figure **5c**): peaks at ca.640.4eV corresponded to Mn^{3+}; the peak at ca.641.5eV corresponded to Mn^{4+}, and satellite peaks appeared at approximately 642.4eV [35]. By calculating the area of different resolved peaks, the Co^{3+}/Co^{2+}molar ratio for the LC-1.0 and LC-1.5 was 0.8 and 2.0. Meanwhile, LM catalysts also showed the similar results. The Mn^{4+}/Mn^{3+}molar ratio for the LM-0.1 and LM-2.0 were 2.2 and 3.2, respectively. The LC-1.5 and LM-2.0 catalysts possessed the higher ratio of $Co^{3+}/Co^{2+}$and Mn^{4+}/Mn^{3+}, which indicated that a high precursor ion concentration was beneficial to increase the valence state of B-site metals on the surface. Furthermore, the high valence states of the B-site metals were more likely to absorb the oxygen species, which can be confirmed by the O 1s XPS analysis.

Figure (**5b,d**) showed the O1s spectra of the catalysts. Abroad and asymmetrical spectrum was observed for each sample and can be classified into three components according to the literature [36,37]: peak situated in the range 528-530eV was attributed to lattice oxygen (O_{latt}), the range 530-532eV was attributed to dissociative oxygen (O_{ads}) on the oxygen vacancy, and the range 532-534eV was attributed to the adsorbed water (O_{wat}) [10]. For the LC-1.5 and LM-2.0 catalysts, the O_{ads} signal shifted upward and became broader, and the O_{ads}/O_{latt} increased significantly, which confirmed that the high ion concentration of precursors leaded to greater surface-adsorbed oxygen species. At the same time, however, lattice oxygen, especially for LC, was significantly reduced. Interestingly, combined with the results of the activity, these two catalysts presented different trends: the activity of LM was consistent with the adsorption of the oxygen content, and the LC was negatively correlated with the adsorption of the oxygen content. Therefore, further exploration was needed. Additionally, the spectra of La3d for each sample showed in supplementary data at BE of825-845 eV and 845-860 eV (Figure **S2**). It can be found that the La 3d spectra of LM-x catalysts had a significant cleavage compared with the LC-x catalysts. The peak cleavage due to the ionization of

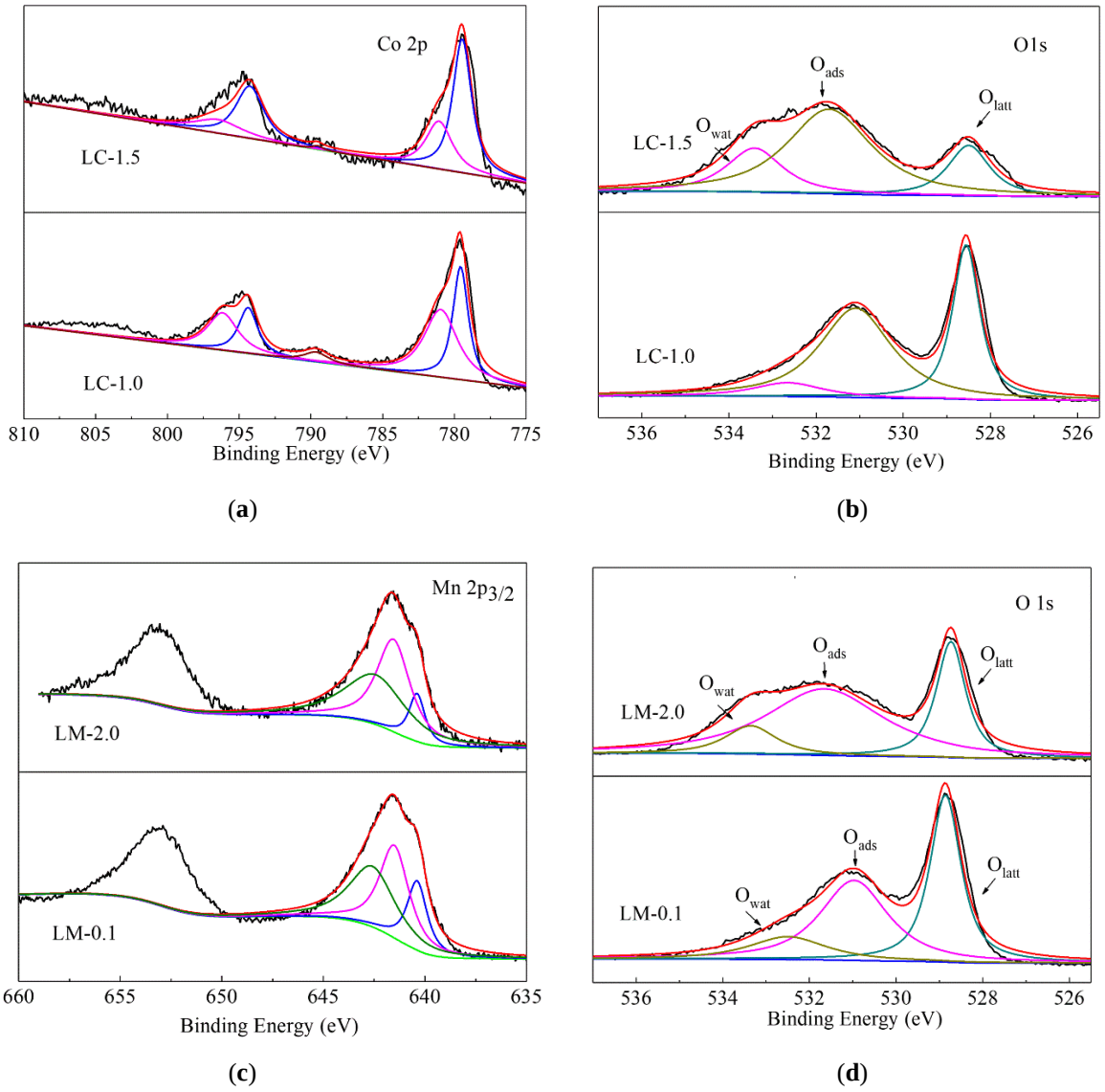

Figure 5: XPS spectra of (**a, b**) LC and (**c, d**) LM catalysts.

Table 3: Surface Element Compositions of LC and LM Catalysts

Catalysts	O_{latt}(%)	O_{ads}(%)	O_{wat}(%)	Molar Ratio[1]			H_2 Comsumption[2]	
				O_{ads}/O_{latt}	Mn^{4+}/Mn^{3+}	Co^{3+}/Co^{2+}	100-500°C	500-900°C
LC-1.0	36.3	55.6	8.1	1.5	-	0.8	0.085	0.186
LC-1.5	17.9	61.0	21.1	3.4	-	2.0	0.098	0.210
LM-0.1	42.0	43.8	14.2	1.0	2.2	-	0.058	0.030
LM-2.0	27.0	61.6	11.4	2.3	3.2	-	0.060	0.086

[1]Molar ratio of O_{ads}/O_{latt}, Mn^{4+}/Mn^{3+} and Co^{3+}/Co^{2+}based on quantitative analysis of XPS.[2]Data based on quantitative analysis of H_2-TPR profiles.

the inner layer electrons of La $3d_{3/2}$ and La $3d_{5/2}$, and then the valence electrons of O 2p coordinated with La were easily transferred to La4f empty orbit. Thus, LM-x catalysts had a strong ability of La-O bond compared with the LC-x catalysts.

3.5. Catalytic Process and DFT Calculation

To confirm the actual reaction process on LC-x and LM-x catalysts, *in situ* DRIFTS experiments were conducted and are shown in (Figure **6**). The IR absorption

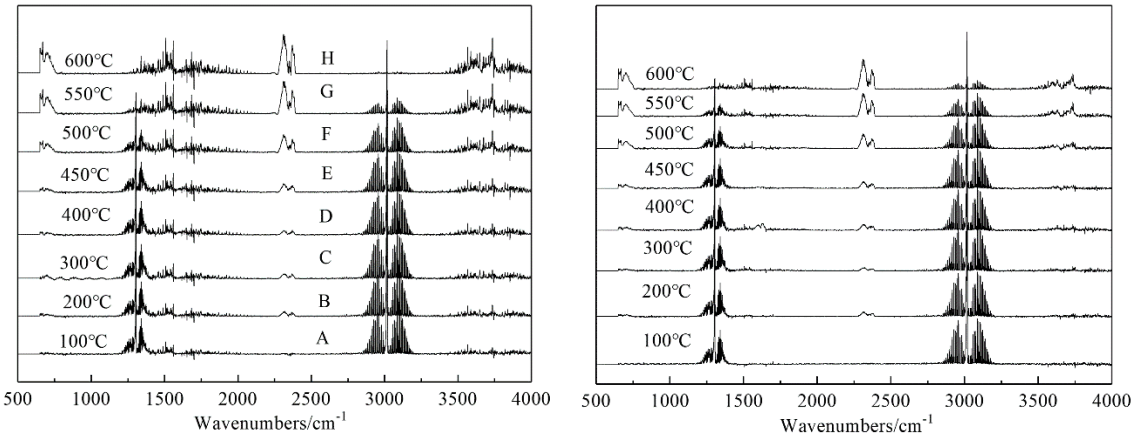

Figure 6: The in-situ DRIFTS spectra of the reaction gas of (**a**) LC-1.0 and (**b**) LM-2.0 catalysts.

bands of the catalysts can be classified into three spectral zones. The first spectral zone displayed the absorption bands centred at 3500-4000 cm^{-1}, which represented the stretching vibration in OH^-. The second spectral zone displayed the narrow peaks around the 3000 cm^{-1} , 1300 cm^{-1} and 1450 cm^{-1}, which can be assigned to the C-H antisymmetric stretching vibration in a free molecule, deformation vibration of C-H bonds [38] and asymmetric stretching in CH_3^- [39], the represented the adsorption of gaseous methane and CH_3^-. The third spectral zone encompasses absorption bands at 2330 cm^{-1} and 2360 cm^{-1}, which can be attributed to the C=O stretching in gaseous carbon dioxide [38]. The fourth spectral zone accounted for remaining vibrations by different species. Specifically, the LC-1.0 catalyst showed intense peaks at 1550 cm^{-1} and 1690 cm^{-1}, which were derived from the strong asymmetric stretching of υ_{as}(C-O), and the absorption peak at 1840 cm^{-1}, which was derived from the υ (C=O) stretching vibration [40]. These peaks were indexed to formate (HCOO-), which provided evidence that CH_4 was easily converse to $HCOO^-$ at the beginning of the catalytic process. However, the LM-2.0 catalyst does not show an $HCOO^-$ peak in low temperatures; instead, it exists in the form of $CH_3\cdot$, and when the temperature reached 550°C, CH_4 rapidly converted into CO_2, while there was a small amount of $HCOO^-$.

To identify the actual reaction process and to explore the reactivity nature, DFT calculations were carried out [41] (Figure **7**). We split the degradation of methane into four steps: methane adsorption, first C-H bond cleavage, water generation and $HCOO^-$ generation. The reaction energy of each step on the B-site and the O-site were both calculated. As was implied by the data, the activation of the first C-H bond was clearly the rate-determining step, which had been commonly recognized in previous research [42]. For LC-*x*, the activation barriers on the Co-site were higher than that calculated for the O-site, which indicated that the degradation of methane was more likely to occur at the lattice oxygen site. However, for LM-*x*, although the adsorption of methane on the O-site was spontaneous (-0.82454eV), the activation barrier of first C-H bond on the Mn-site (0.026445eV) was much lower than that on the O-site (5.120013eV), which suggested that the degradation of methane more easily occurred on the Mn-site. The DFT simulation results well verified the conclusion of the above characterization. For LC, the lattice oxygen content determines the activity, while for LM, the content of high-valence Mn is closely related to the activity. This is consistent with the characterization results of XPS and TPR.

4. CONCLUSIONS

In this study, $LaCoO_3$ and $LaMnO_3$ perovskite-type catalysts were prepared by different ion concentrations of precursors. The structures, morphologies, surface characteristics, adsorption properties, catalytic activities and mechanisms of methane catalytic oxidation were studied. As the ion concentrations of precursors increased, the porosity catalysts became more agglomerate, and the SSA decreased. Meanwhile, the proportion of surface high-valence states of B-site ions increased, thus leading to more adsorbed surface oxygen species. The two kinds of catalysts showed almost opposite correlations between x and the catalytic activity. Therefore, we had thoroughly studied its reaction mechanism. *In situ* DRIFTS experiments

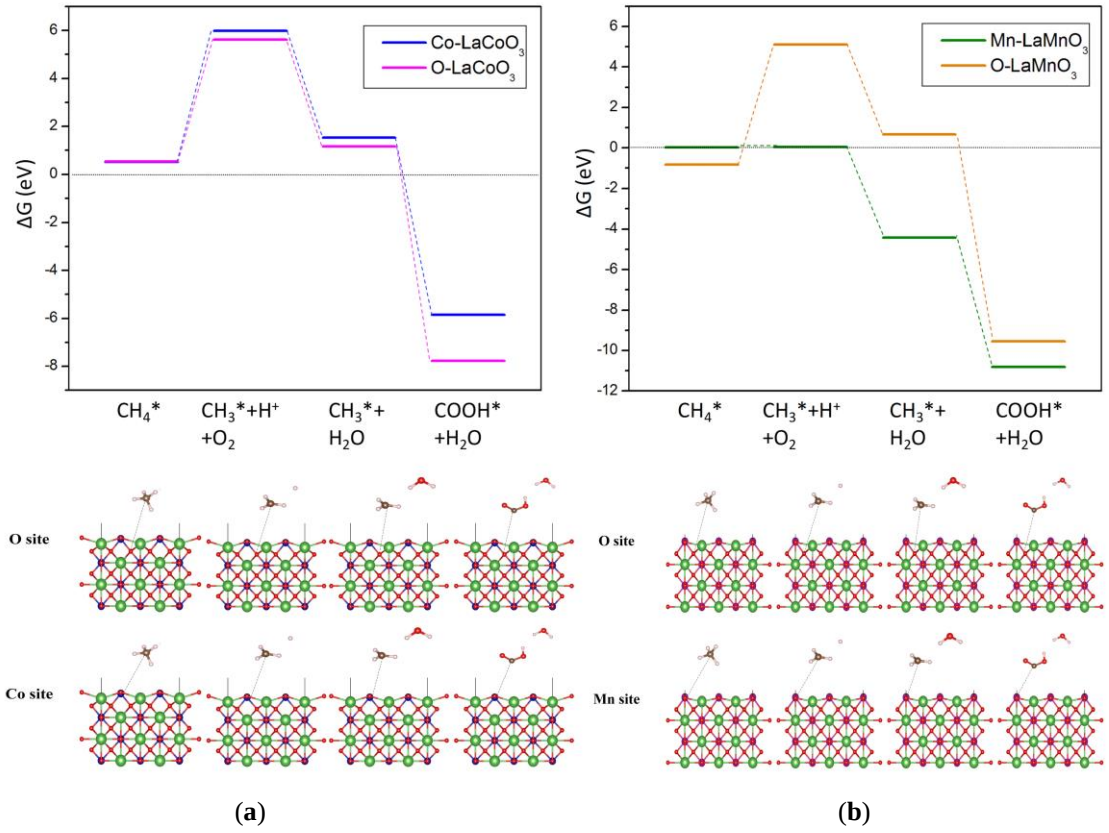

Figure 7: Theoretical identification of free energy diagrams of CH_4 oxidation on (**a**) LC and (**b**) LM catalysts. Color code: La: green, Co: blue, Mn: purple, O: red, C: brown, H: white.

verified the difference in the intermediate process of the reaction, and XPS combined with DFT calculation proved that for LC, the degradation of methane is more prone to occur at the O-site, or the lattice oxygen, so the catalytic activity of LC was positively correlated to the content of lattice oxygen. For LM, although methane was more likely to be adsorbed at the O-site, the first C-H bond broke and extremely easily occurred at the Mn-site. Therefore, the activity of LM was related to the existence of high-valence Mn or the surface adsorption of oxygen.

FUNDING

This research was funded by the Ministry of Education Blue Fire Program (No. CXZJH201717), Shijiazhuang Science and Technology Department (No. 181240243A and 191240273A) and the Hebei Provincial Department of Science and Technology (No. 19943816G).

CONFLICTS OF INTEREST

The authors declare no conflict of interest.

REFERENCES

[1] Wang C, Yang S, Li X. Simulation of the hazard arising from the coupling of gas explosions and spontaneously combustible coal due to the gas drainage of a gob. Proc Safety Environ Protec. 2018; 118: 296-306. https://doi.org/2018.06.028 0957-5820

[2] Liu F, Sang Y, Ma H. Nickel oxide as an effective catalyst for catalytic combustion of methane. J Nat Gas Sci Eng. 2017; 41: 1-6. https://doi.org/10.1016/j.jngse.2017.02.025

[3] Messaoudani ZI, Rigas F, Hamid MDB, Hassan CRC. Hazards, safety and knowledge gaps on hydrogen transmission via natural gas grid: A critical review. Int J Hydrogen Energy 2016; 41: 17511-17525. https://doi.org/10.1016/j.ijhydene.2016.07.171

[4] Thiruvengadam A, Besch M, Padmanaban V, Pradhan S, Demirgok B. Natural gas vehicles in heavy-duty transportation-A review, Energy Policy 2018; 122: 253-259. https://doi.org/10.1016/j.enpol.2018.07.052

[5] Jiang X, Mira D, Cluff DL. The combustion mitigation of methane as a non-CO_2 greenhouse gas. Prog Energy Combust Sci. 2018; 66: 176-199. https://doi.org/10.1016/j.pecs.2016.06.002

[6] Yang J, Guo Y. Nanostructured perovskite oxides as promising substitutes of noble metals catalysts for catalytic combustion of methane. Chinese Chemical Letters 2018; 29: 252-260. DOI: 10.1016/j.cclet.2017.09.013

[7] Lei Y, Li W, Liu Q. Typical crystal face effects of different morphology ceria on the activity of Pd/CeO_2 catalysts for lean methane combustion. Fuel 2018; 233: 10-20. https://doi.org/10.1016/j.fuel.2018.06.035

[8] Okal J, Zawadzki M, Baranowska K. Methane combustion over bimetallic Ru-Re/γ-Al_2O_3 catalysts: Effect of Re and pretreatments. Appl Catal B. 2016; 194: 22-31. https://doi.org/10.1016/j.apcatb.2016.04.038

[9] Hong E, Kim C, Lim DH. Catalytic methane combustion over Pd/ZrO_2 catalysts: Effects of crystalline structure and textural properties. Appl Catal B. 2018; 232: 544-552. https://doi.org/10.1016/j.apcatb.2018.03.101

[10] Chin YH, Buda C, Neurock M, Iglesia E. Consequences of metal-oxide interconversion for C-H bond activation during CH_4 reactions on Pd catalysts. J Am Chem Soc. 2013; 135: 15425-15442. https://doi.org/10.1021/ja405004m

[11] Liotta LF, Carlo G, Di Pantaleo G, Deganello G. Catalytic performance of Co_3O_4/CeO_2 and $Co_3O_4/CeO_2–ZrO_2$ composite oxides for methane combustion: Influence of catalyst pretreatment temperature and oxygen concentration in the reaction mixture. Applied Catalysis B: Environmental, 2007; 70: 314-322. https://doi.org/10.1016/j.apcatb.2005.12.023

[12] Yang Q, Liu G, Liu Y. Perovskite-Type Oxides as the Catalyst Precursors for Preparing Supported Metallic Nanocatalysts: A Review. Industrial & Engineering Chemistry Research. 2017; 57: 1-17. https://doi.org/10.1021/acs.iecr.7b03251

[13] Zhu H, Zhang P, Dai S. Recent Advances of Lanthanum-Based Perovskite Oxides for Catalysis. ACS Catalysis 2015; 5: 6370-6385. https://doi.org/10.1021/acscatal.5b01667

[14] Zhang D, Tan Q, Meng X, Weng ZW. Structural modification of $LaCoO_3$ perovskite for oxidation reactions: The synergistic effect of $Ca^{2+}$and Mg^{2+}co-substitution on phase formation and catalytic performance. Applied Catalysis B: Environ.. 2015; 172: 18-26. http://dx.doi.org/10.1016/j.apcatb.2015.02.006

[15] Arandiyan H. Methane Combustion over Lanthanum-based Perovskite Mixed Oxides. 2015; ISBN 978-3-662-46990-3. DOI: 10.1007/978-3-662-46991-0.10,16-17

[16] Mishra A, Prasad R. Preparation and application of perovskite catalysts for diesel soot emissions control: an overview. Catalysis Reviews 2014; 56: 57-81. https://doi.org/10.1080/01614940.2014.866438

[17] Wang J, Ren Y, Wang F, Zhang X, Liu Y, Guo GL. Nanocasted Synthesis of Mesoporous $LaCoO_3$ Perovskite with Extremely High Surface Area and Excellent Activity in Methane Combustion. J Phys Chem C. 2008; 112: 15293-15298. https://doi.org/10.1021/jp8048394

[18] Wang L. Ma. NO oxidative activity of mesoporous $LaMnO_3$and $LaCoO_3$perovskite nanoparticles by facile molten-salt synthesis. New J Chem. 2019; 43: 2974-2980. DOI: 10.1039/C8NJ04590A

[19] Hou L, Zhang H, Dong L, Zhang L, Duprez D, Royer S. A simple non-aqueous route to nano-perovskite mixed oxides with improved catalytic properties. Catal. Today. 2017. 287: 30-36. https://doi.org/10.1016/j.cattod.2017.01.047

[20] Spinicci R, Faticanti M, Marini P, De Rossi S, Porta P. Catalytic activity of $LaMnO_3$ and $LaCoO_3$ perovskites towards VOCs combustion. Journal of Molecular Catalysis A: Chem .2003; 197: 147-155. https://doi.org/10.1016/S1381-1169(02)00621-0

[21] Si W, Wang Y, Zhao S, Hu F, Li J. A Facile Method for in Situ Preparation of the $MnO_2/LaMnO_3$ Catalyst for the Removal of Toluene. Environ Sci Technol. 2016; 50: 4572-4578. https://doi.org/10.1021/acs.est.5b06255

[22] Wang Y, Arandiyan H, Scott J, *et al*. High Performance Au–Pd Supported on 3D Hybrid Strontium-Substituted Lanthanum Manganite Perovskite Catalyst for Methane Combustion. ACS Catal. 2016; 6: 6935-6947. https://doi.org/10.1021/acscatal.6b01685

[23] Campagnolia AE, Tavaresb LF, Rossettia I, *et al*. Effect of preparation method on activity and stability of $LaMnO_3$ and $LaCoO_3$ catalysts for the flameless combustion of methane. Appl Catal B. 2005; 55: 133-139. https://doi.org/10.1016/j.apcatb.2004.07.010

[24] Zhu J, Sun X, Wang Y, *et al*. Solution-phase synthesis and characterization of perovskite$LaCoO_3$nanocrystals via a co-precipitation Route. J Rare Earths 2007; 25: 601-604. https://doi.org/10.1016/S1002-0721(07)60570-5

Gao Z, Wang R. Catalytic activity for methane combustion of the perovskite-type $La_{1-x}Sr_xCoO_{3-\delta}$ oxide prepared by the urea decomposition method. Applied Catalysis B: Environl. 2010; 98: 147-153. https://doi.org/10.1016/j.apcatb.2010.05.023

[25] Natile M, Ugel E, Maccato C, Glisenti A. $LaCoO_3$: effect of synthesis conditions on properties and reactivity. Applied Catalysis B: Environ. 2007; 72(3): 351-362. https://doi.org/10.1016/j.apcatb.2006.11.011

[26] Arandiyan H, Chang H, Liu C, Peng Y, Li J. Dextrose-aided hydrothermal preparation with large surface area on 1D single-crystalline perovskite $La_{0.5}Sr_{0.5}CoO_3$ nanowires without template: Highly catalytic activity for methane combustion. Journal of Molecular Catalysis A: Chem. 2013; 378: 299-306. https://doi.org/10.1016/j.molcata.2013.06.019

[27] Ghiasi E, Malekzadeh A, Ghiasi M. Moderate concentration of citric acid for the formation of $LaMnO_3$ and $LaCoO_3$ nano-perovskites. J Rare Earths 2013; 31: 997-1002. https://doi.org/10.1016/S1002-0721(12)60393-7

[28] Kresse G, Furthmuller J. Efficient iterative schemes for ab initio total-energy calculations using a plane-wave basis set. Phys. Rev. B: Condens. Matter Mater Phys. 1996; 54: 11169-11186. https://doi.org/10.1103/physrevb.54.11169

[29] Kresse G, Furthmuller J. Efficiency of ab-initio total energy calculations for metals andsemiconductors using a plane-wave basis set. J Comput Mater Sci. 1996; 6: 15. DOI: https://doi.org/10.1016/0927-0256(96)00008-0

[30] Perdew JP, Burke K, Ernzerhof M. Generalized Gradient Approximation Made Simple. Phys Rev Lett. 1996; 77: 3865-3868. https://doi.org/10.1103/physrevlett.77.3865

[31] Navarro RM, Alvarez-Galvan MC, Villoria JA, *et al*. Effect of Ru on $LaCoO_3$ perovskite-derived catalyst properties tested in oxidative reforming of diesel. Appl Catal B. 2007; 73: 247-258. https://doi.org/10.1016/j.apcatb.2006.12.013

[32] Hou L, Zhang H, Dong L, *et al*. A simple non-aqueous route to nano-perovskite mixed oxides with improved catalytic properties. Catal Today 2017; 287: 30-36. https://doi.org/10.1016/j.cattod.2017.01.047

[33] Ren Q, Feng Z, Mo S, *et al*. 1D-Co_3O_4, 2D-Co_3O_4, 3D-Co_3O_4 for catalytic oxidation of toluene. Catal Today 2019; 332: 160-167. https://doi.org/10.1016/j.cattod.2018.06.053

[34] Liu Y, Dai H, Deng J, *et al*. Controlled generation of uniform spherical $LaMnO_3$, $LaCoO_3$, Mn_2O_3, and Co_3O_4 nanoparticles and their high catalytic performance for carbon monoxide and toluene oxidation. Inorg Chem. 2013; 52: 8665-8676. https://doi.org/10.1021/ic400832h

[35] Gao Z, Wang H, Ma H, Li Z. Preparation and characterization of the non-stoichiometric La-Mn perovskites. J Alloys Compd. 2015; 646: 73-79. https://doi.org/10.1016/j.jallcom.2015.06.044

[36] Zhu J, Li H, Zhong L, *et al*. Perovskite Oxides: Preparation, Characterizations, and Applications in Heterogeneous Catalysis. ACS Catal. 2014; 4: 2917-2940. https://doi.org/10.1021/cs500606g

[37] Schmal M, Souza M, Alegre V, *et al*. Methane oxidation - effect of support, precursor and pretreatment conditions - *in*

situ reaction XPS and DRIFT. Catal Today 2006; 118: 392-401. https://doi.org/10.1016/j.cattod.2006.07.026

[38] Wang Y, Arandiyan H, Scott J, *et al*. High Performance Au–Pd Supported on 3D Hybrid Strontium-Substituted Lanthanum Manganite Perovskite Catalyst for Methane Combustion. ACS Catal. 2016; 6: 6935-6947. https://doi.org/10.1021/acscatal.6b01685

[39] Jodłowski PJ, Jedrzejczyk RJ, Chlebda D, Gierada M, Łojewska J. *In situ* spectroscopic studies of methane catalytic combustion over Co, Ce, and Pd mixed oxides deposited on a steel surface. J Catal. 2017; 350: 1-12. https://doi.org/10.1016/j.jcat.2017.03.022

[40] Glisenti A, Vittadini A. On the Effects of Doping on the Catalytic Performance of (La,Sr)CoO_3. A DFT Study of CO Oxidation. Catalysts 2019; 9: 312. https://doi.org/10.3390/catal9040312

[41] Polo-Garzon F, Fung V, Liu X, *et al*. Understanding the Impact of Surface Reconstruction of Perovskite Catalysts on CH_4 Activation and Combustion. ACS Catal. 2018; 8: 10306-10315. https://doi.org/10.1021/acscatal.8b02307

Received on 14-05-2020 Accepted on 12-06-2020 Published on 25-09-2020

DOI: https://doi.org/10.15377/2410-3624.2020.07.2